Focused-Laser-Enabled p–n Junctions in Graphene Field-Effect Transistors

Young Duck Kim,[†] Myung-Ho Bae,[‡] Jung-Tak Seo,[§] Yong Seung Kim,[∥] Hakseong Kim,[△] Jae Hong Lee,[∥] Joung Real Ahn,[§,⊥] Sang Wook Lee,[△] Seung-Hyun Chun,[∥] and Yun Daniel Park[†,*]

[†]Center for Subwavelength Optics and Department of Physics and Astronomy, Seoul National University, 1 Gwanak-ro, Gwanak-gu, Seoul, 151-747, Republic of Korea, [‡]Korea Research Institute of Standards and Science, 267 Gajeong-ro, Yuseong-gu, Daejeon, 305-340, Republic of Korea, [§]Department of Physics and [⊥]SAINT and Center for Integrated Nanostructure Physics, Institute for Basic Science, Sungkyunkwan University, 300 Cheoncheon-dong, Jangan-gu, Suwon, 440-746, Republic of Korea, [∥]Department of Physics and Graphene Research Institute, Sejong University, 209 Neungdong-ro, Gwangjin-gu, Seoul, 143-747, Republic of Korea, and [△]Division of Quantum Phase and Quantum Devices, School of Physics, Konkuk University, Seoul, 143-701, Republic of Korea

ABSTRACT

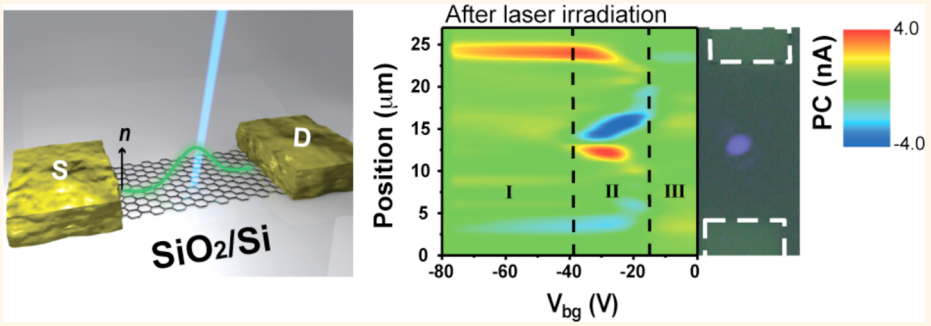

With its electrical carrier type as well as carrier densities highly sensitive to light, graphene is potentially an ideal candidate for many optoelectronic applications. Beyond the direct light–graphene interactions, indirect effects arising from induced charge traps underneath the photoactive graphene arising from light–substrate interactions must be better understood and harnessed. Here, we study the local doping effect in graphene using focused-laser irradiation, which governs the trapping and ejecting behavior of the charge trap sites in the gate oxide. The local doping effect in graphene is manifested by large Dirac voltage shifts and/or double Dirac peaks from the electrical measurements and a strong photocurrent response due to the formation of a p–n–p junction in gate-dependent scanning photocurrent microscopy. The technique of focused-laser irradiation on a graphene device suggests a new method to control the charge-carrier type and carrier concentration in graphene in a nonintrusive manner as well as elucidate strong light–substrate interactions in the ultimate performance of graphene devices.

KEYWORDS: graphene · focused laser · p–n junction · photocurrent · charge trap · local doping effect

Graphene is an atomically thin, two-dimensional carbon material, whose honeycomb bonding structure provides unique electrical,[1,2] optical,[3] and mechanical properties.[4] A zero band gap with a linear dispersion relationship makes the graphene-based, field-effect transistor (GFET) and its operating characteristics highly sensitive to minute variations in carrier type and density.[5–7] Thus, spatial modulation of the doping profile, such as the p–n junction in graphene, is of high interest in fundamental studies, including those concerning the Veselago lens,[8] Klein tunneling,[9] graphene superlattice,[10] and post-CMOS application devices, such as high-frequency photodetectors,[11–13] energy-harvesting devices,[14–16] and nonvolatile memory.[17–19] A common underlying principle of the above graphene-based optoelectronic device applications is dependence of electrical current to light irradiation, light–graphene interactions. On the other hand, it has been found that small intensity of visible laser irradiation alters the charge neutral point and Raman shift of graphene due to charge traps under graphene.[20]

Charge-carrier transfer between graphene and the charge trap sites in gate oxide induces a local doping effect in the graphene channel.[17–19] The charge trap

* Address correspondence to parkyd@phya.snu.ac.kr.

Received for review March 1, 2013 and accepted June 19, 2013.

Published online June 20, 2013
10.1021/nn402354j

sites in the oxide that are within 4–8 nm[21] of the interface are typically impurity- and defect-induced Coulomb attractive centers that are positively charged (N_D^+).[22,23] The trap sites are capable of electron trapping ($N_D^+ + e^- \rightarrow N_D$) and ejecting ($N_D \rightarrow N_D^+ + e^-$) by Schottky emission[24] and the trapped-charge density (N_D) is indicated by hysteretic behavior or a shift of the Dirac voltage (V_{Dirac}),[25–27] which is a gate voltage corresponding to the maximum resistance. Previous studies have been conducted to characterize the charge-carrier transfer between graphene and the charge trap sites at the SiO_2/graphene interface by electric field,[17,18] chemical dopant,[28–31] and hot carriers.[32] Among the numerous studies, there is little information on strong light–substrate interaction induced doping effects in graphene devices, despite their important role in the performance and characterization of graphene-based devices such as photodetectors and bolometers.[33] Thus, the measurement of strong light–substrate interaction effects in graphene devices allows one not only to understand the optically excited charge-carrier transfer process but also to manipulate doping effects for advanced graphene-based optoelectronic devices.

Here, we present the spatially modulated doping effect in graphene on a SiO_2/Si substrate by locally focused-laser irradiation, which induces charge transfer between the charge trap sites and the graphene. A strong interaction between the laser irradiation and the charge trap site alters the local electrostatic potential of the substrate *via* the optically induced trapped charges in the gate oxide. As a result, V_{Dirac} of the GFET, which is sensitive to the local doping profile, shifts correspondingly. The spatial doping distribution and the local doping levels in the GFET are visualized using gate-dependent scanning photocurrent microscopy (SPM).[34–36] We also estimate the energy scales related to the trap site based on a charge-transfer process, ~2.6 eV corresponding to ~470 nm wavelength light, which is consistent with the charge-ejecting rates for different photon energies. We believe that the laser-irradiation-induced controllable doping level and the spatial profile in the GFET have great potential to realize extraordinary graphene-based optoelectronic devices.

RESULTS AND DISCUSSION

GFETs are fabricated with single-layer graphene prepared using both chemical vapor deposition (CVD)[37] and mechanical exfoliation on SiO_2 (300 nm)/Si (highly p-doped) substrate. Graphene channels are patterned using an O_2 plasma process. After e-beam lithography and evaporation, the source and drain electrodes of Cr/Au (10/40 nm) are prepared on the graphene. The highly p-doped Si substrate is used as a global back-gate electrode. The CVD GFET channel dimensions are 3 μm in width and have lengths of 2, 8, 20, 40, and 50 μm; similarly, the mechanically exfoliated GFET channels have varying widths and lengths. To minimize the effect of charge trapping and ejecting by electrically generated energetic carriers,[32] electrical measurements such as the resistance as a function of the back-gate voltage (R–V_{bg}) and time are performed with a 100 mV source–drain bias (V_{SD}) in a vacuum (<10^{-4} Torr) at room temperature after laser turn-off (R–V_{bg} curve). Photocurrent (PC) measurements are performed using a 633 nm–250 μW He–Ne laser without source–drain bias. In addition, to reduce any interaction with impurities on/below the graphene channel, we use current annealing to prepare the GFET (see Figure S1 in the Supporting Information). Figure 1a presents a schematic of the GFET on the SiO_2/Si substrate and laser irradiation on the graphene channel.

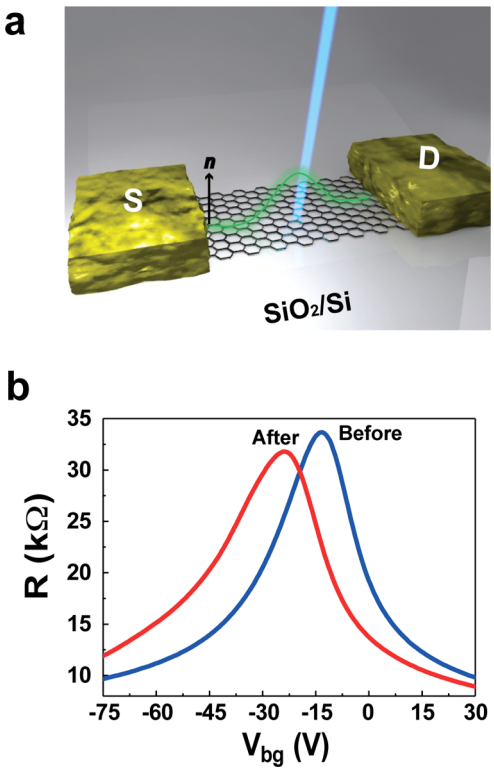

Figure 1. (a) Schematic of a GFET on a SiO_2/Si substrate and the laser irradiation on the center of the graphene channel. Laser irradiation modulates the local carrier concentration of graphene by governing the local charge trap sites in the gate oxide. The green line represents the expected carrier concentration profile along the GFET channel. (b) R–V_{bg} curves for a 20-μm-long GFET (gate voltage sweep from negative to positive voltage). The red (blue) curve is obtained after (before) 400 s of 442 nm–600 μW laser irradiation onto the center of graphene with V_{bg} = −50 V. Both measurements are performed under "dark" conditions.

To explore the doping effect from the focused-laser irradiation onto the GFET, we measure R–V_{bg} for a 20-μm-long GFET (back-gate voltage sweep direction induced hysteresis and the Dirac-voltage shift (ΔV_{Dirac}) for the opposite sweep directions is smaller than 5 V, as shown in Figure S9 in the Supporting Information). Figure 1b shows the R–V_{bg} curve before (blue curve) and after (red curve) 442 nm–600 μW laser irradiation

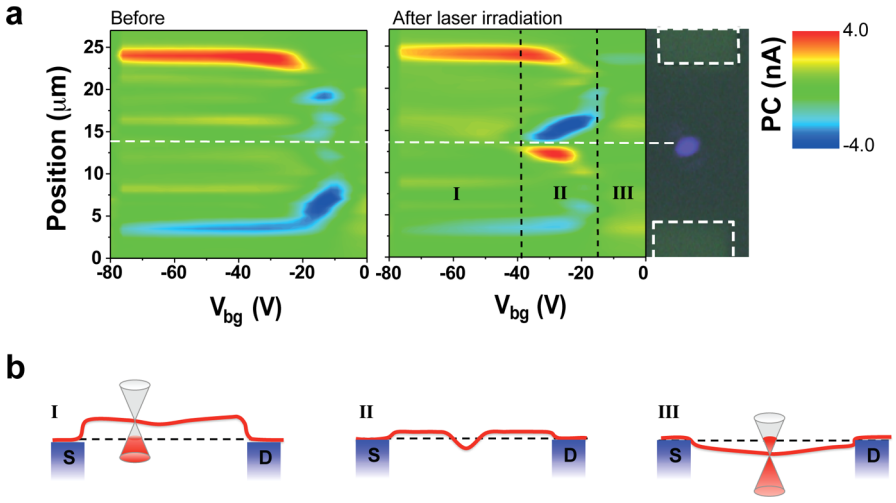

Figure 2. (a) Gate-dependent SPM image of a 20-μm-long GFET along the graphene channel. The SPM image on the right (left) is acquired after (before) the 442 nm−600 μW laser irradiation onto the center of the GFET without V_{sd}. Strong PC modulation is observed at the center of the GFET in region II after laser irradiation. The far right image is the optical microscope image of the GFET with a 442 nm laser focused at the center, and focused laser spot size is about 1 μm. (b) Expected schematic of the band bending in the GFET after 442 nm laser irradiation with different gate voltage regions: (I) -80 V < V_{bg} < -38 V, (II) -38 V < V_{bg} < -15 V, (III) -15 V < V_{bg}. The dashed line represents the Fermi energy level along the GFET, and the solid red curve represents the local Dirac point of graphene.

onto the center of the graphene channel for 400 s with $V_{bg} = -50$ V (see Supporting Information Figure S2 for the resistance variation as a function of time). After the laser irradiation, the Dirac voltage shifts as $\Delta V_{Dirac} = -9.5$ V (as shown in Figure 1b), which indicates an n-type doping effect to graphene. (See also Supporting Information Figures S3 and S4, which present a more detailed set of data for a large V_{Dirac} shift ($\Delta V_{Dirac} \approx -60$ V) for various V_{bg} and laser intensities and for the resistance varying over time. Furthermore, the efficiency of charge-carrier transfer between graphene and charge trap sites in the gate oxide depends on applied gate voltage during focused-laser irradiation, as shown in Figures S3 and S4.) We assume that the optically excited electrons transfer from the trap sites to the graphene, while the positive charge carriers remain trapped in the trap sites in the gate oxide. These positively charged trap sites lead to a gating effect in the graphene through capacitive coupling and modulate the local carrier concentration of the graphene channel. From the direction and the magnitude of the shift, we can surmise that the laser-irradiation-induced trapped-charge density (N_D) is approximately 6.9×10^{11} cm^{-2} (this value is estimated from $\Delta V_{Dirac} = -9.5$ V).

To verify the laser-irradiation-induced doping location and concentration, as well as the size of the doped segment formation, we perform gate-dependent SPM on GFETs. For the photocurrent microscopy on a 20-μm-long GFET, we use a 633 nm−250 μW He−Ne laser to induce the photocarriers in the graphene channel without any source−drain bias. The PC is obtained using a lock-in measurement technique with an optical chopper (1.45 kHz). We measure the gate-dependent PC and map the PC along the graphene channel length for various values of V_{bg} before (Figure 2a, left) and after (Figure 2a, right) 400 s of 442 nm−600 μW laser irradiation. The 442 nm laser irradiation is used to optically eject the trapped charges (*i.e.*, $N_D \rightarrow N_D^+ + e^-$). The regions near the source and drain electrodes (corresponding to the dashed, rectangular boxes in the far right of Figure 2a) show a clear positive and a clear negative PC by the 633 nm laser, respectively, regardless of the 442 nm laser irradiation. This result is related to the doping effect from band bending *via* the metal−contact work functions and is consistent with previously reported observations.[34−36,38]

After the 442 nm laser irradiation onto the center of the graphene channel, we observe a strong PC modulation by the 633 nm laser with respect to the 442 nm laser irradiated spot position, as shown in gate-voltage region II of the SPM image (right) in Figure 2a. The strong PC response near the center of the GFET is attributed to both photovoltaic and photothermoelectric effects (bolometric effect[33,39,40] does not contribute to PC response at any gate voltage without source−drain bias in graphene) near the local trapped-charge density (N_D) region. The local density modulation is induced by the 442 nm laser and results in the formation of the p−n−p junction in the graphene with a modest gate voltage (-38 V < V_{bg} < -15 V; region II in Figure 2a) by a band bending in the graphene channel (region II in Figure 2b). The schematic of the band bending in graphene after the 442 nm laser irradiation is shown in Figure 2b for three regions of V_{bg} (I, II, and III). The electrostatically induced large carrier concentration in graphene suppresses the laser-irradiation-induced local doping effect in regions

I and III in Figure 2a and b, respectively. However, when V_{bg} is near V_{Dirac} of the graphene channel, the 442 nm laser-irradiation-induced local doping effect becomes a dominant source for the trapped-charge density modulation and results in the p−n−p junction, which is indicated by the strong PC response (region II in Figure 2a and b). The spatially sharp p−n junction in GFET is approximately 500 nm at $V_{bg} = -38$ V. Furthermore, the spatial region for the strong PC modulation at the center of the channel is extended when V_{bg} varies from −38 V to −15 V in the SPM image (right) of Figure 2a. The crossing points of the p−n and n−p junctions in Figure 2b-II spatially move away from each other along the graphene channel when V_{bg} increases in the gate region. Because the PC is enhanced at the region where the carrier type of graphene is crossed (p−n junction, see Figure 2b-II), the above crossing behavior with respect to V_{bg} could explain this observation. We also observe two strong PC modulation regions on the graphene channel when we focus the 442 nm−600 μW laser at two different points in the 40-μm-long graphene channel (see Supporting Information Figure S5), which results in the p−n−p−n−p junction. From these results, we can confirm that the position of the focused-laser spot determines the location and the number of p−n junctions in graphene.

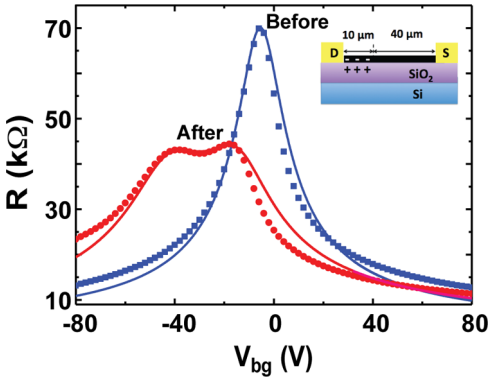

Figure 3. $R-V_{bg}$ curves for a 50-μm-long GFET (gate voltage sweep from negative to positive voltage). The red (blue) scattered points are obtained after (before) 20 min of 442 nm−1 mW laser irradiation with $V_{bg} = -50$ V near the drain electrode. The theoretical calculation of pristine graphene (blue curve) and the 10 μm (effective length) locally doped graphene near the drain electrode (red curve) is well fitted.

To further illustrate and study the 442 nm laser irradiation induced p−n junction in GFET, we conduct a series of electrical measurements. We measure and plot the $R-V_{bg}$ curves for a 50-μm-long GFET to isolate a single dominant p−n junction. We focus the 442 nm−1 mW laser with $V_{bg} = -50$ V near the drain electrode of GFET for 20 min to make a strong and stable *n*-type-doped region along the graphene channel. The laser-irradiation-induced local doping effect and the formation of a p−n junction in graphene are clearly indicated by the two resistance peaks in the $R-V_{bg}$ curve, as shown in Figure 3 (red circle); in this figure, the blue square represents the behavior before laser irradiation. The two local maximum resistances in the $R-V_{bg}$ curve indicate that a p−n junction is formed in the graphene channel.[20,32] The SPM image of the channel after the 442 nm laser irradiation (see Supporting Information Figure S6) shows the PC modulation over a length of approximately 10 μm near the drain electrode, which corresponds to the length of the locally doped region in the graphene. To reproduce these $R-V_{bg}$ curves theoretically, we divide the graphene channel into two sections (see the inset of Figure 3) of $L_1 = 40$ μm (nondoped region) and $L_2 = 10$ μm (locally doped region). The total resistance is defined by[41]

$$R = R_p + 2R_c + R_{S1}\frac{L_1}{W} + R_{S2}\frac{L_2}{W} \quad (1)$$

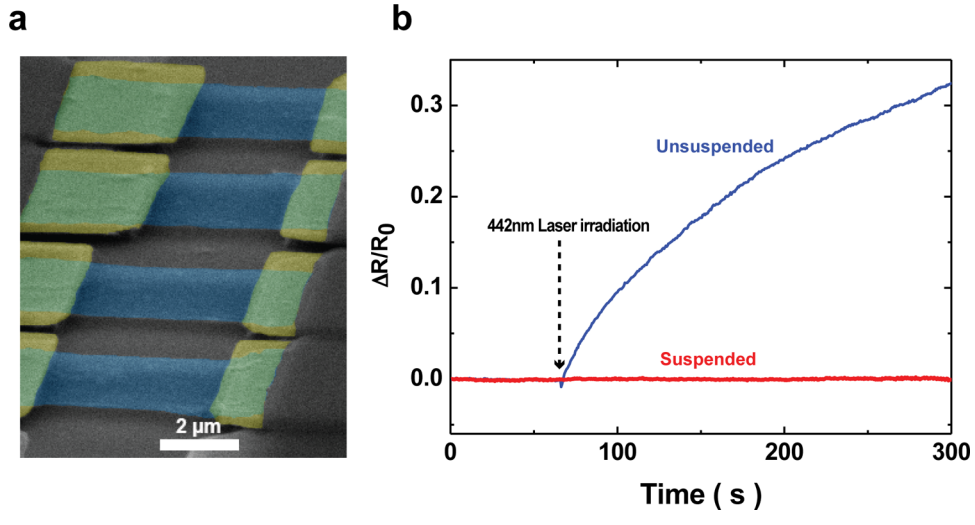

Figure 4. (a) SEM image of suspended graphene structures. (b) Resistance ratio ($\Delta R/R_0$) of a 5-μm-long suspended GFET (red curve, the third one from the top in (a)) and 8-μm-long unsuspended GFET (blue curve) as a function of time with a 442 nm−250 μW laser irradiated onto the center of the each of graphene channels with zero gate voltage. R_0 is initial resistance of the GFETs. Laser-induced doping effect is dominant at the unsuspended GFET due to trapped charges in the gate oxide.

where $R_S = 1/[e\mu_0(n + p)]$ is the sheet resistance of the graphene; μ_0 is the zero-field mobility; $n(p)$ is the electron (hole) carrier density per unit area, which is defined by $n,p = (1/2)\{\mp C_{ox}(V_{Dirac} - V_{bg})/e + ([C_{ox}(V_{Dirac} - V_{bg})/e)]^2 + 4n_i^2)^{1/2}\}$; $C_{ox} = \varepsilon_{ox}\varepsilon_0/t_{ox}$ is the capacitance per unit area; $\varepsilon_{ox} = 3.9$ is the dielectric constant of SiO_2; ε_0 is the vacuum permittivity; $n_i = (n_{th} + n_p)$ is the intrinsic carrier density, which is composed of the thermally excited carrier density, $n_{th} = (\pi/6)(k_BT/\hbar v_F)^2$ and the puddle density, n_p; T is the base temperature; and v_F is the Fermi velocity of charges in graphene.[42] For environmental resistances, we consider the contact resistance $R_c = \rho_c/(WL_T)\coth(L_c/L_T)$ and the metal pad resistance, R_p. Here, ρ_c is the contact resistivity per unit area, L_c is the overlapping length of metal on graphene, and $L_T = (\rho_c/R_S)^{1/2}$ is the current-transfer length at the contact region.

At first, we fit the $R-V_{bg}$ curve before irradiation (experimental data: blue scattered points; fit result: blue solid curve), as shown in Figure 3. The parameters that we use are as follows: $L_1 = 50\ \mu$m, $L_2 = 0\ \mu$m, $\rho_c = 600\ \Omega\ \mu$m^2, $R_p = 2.5$ kΩ, $n_{th} = 8 \times 10^{10}$ cm^{-2} at $T = 300$ K, $n_p = 2.45 \times 10^{11}$ cm^{-2}, and $\mu_0 = 2400$ cm^2 V^{-1} s^{-1}. For the $R-V_{bg}$ curve (red scattered points) after laser irradiation, with $L_1 = 40\ \mu$m and $L_2 = 10\ \mu$m, we obtain the best fit result (red solid curve) using $\mu_{01} = 3100$ cm^2 V^{-1} s^{-1} and $\mu_{02} = 680$ cm^2 V^{-1} s^{-1} with $n_{p1} = 4.2 \times 10^{11}$ cm^{-2} and $n_{p2} = 5 \times 10^{11}$ cm^{-2}. From the PC image and theoretical calculation, we estimate that the length of the doped region resulting from laser irradiation is approximately 10 μm, which is similar to that observed *via* the SPM image in Figure S6 in the Supporting Information. Thus, strong laser intensity and long irradiation time can also affect the doping concentration and the size of the doped segment in graphene.

To verify the role of gate oxide in the laser-irradiation-induced doping effect of GFETs, we measure the resistance variation as a function of time of suspended and unsuspended graphene with 442 nm−250 μW laser irradiation with zero gate voltage, as shown in Figure 4. The fabrication procedures of suspended graphene are described in the Supporting Information. The focused 442 nm laser was irradiated onto the center of graphene, and we did not observe any noticeable doping effect from the suspended device with zero and nonzero gate voltage, while the unsuspended device showed a large doping effect with zero gate voltage, as shown in Figure 4b. Thus, this experimental result confirms that the role of the gate oxide is very important in optically assisted charge transfer in GFETs.

Both the optically assisted charge transfer in GFET and the trapped-charge density depend on the irradiated photon energy, applied electrical gate voltage, and the energy barrier heights of the charge trap sites.[43−45] To investigate the charge-transfer dynamics in GFET, we compare the resistance ($V_{SD} = 100$ mV) as a function of time with different irradiated energies of 2.81 eV (442 nm) and 1.96 eV (633 nm); this irradiation

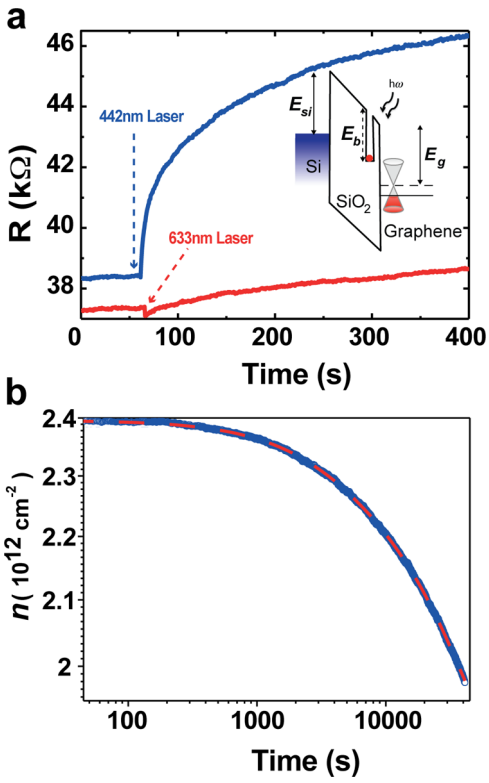

Figure 5. (a) Resistance (R) of a 40-μm-long GFET as a function of time with different irradiated photon energies. The 2.81 eV (442 nm, blue dot) and 1.96 eV (633 nm, red dot) lasers with equal intensities of 600 μW are irradiated onto the center of the graphene channel with a fixed electrical gate voltage ($V_{bg} = -50$ V). The inset is the schematic of the band diagram of the optically assisted charge-transfer process in GFET with a negative electrical gate voltage. Here the energy difference between the bottom of the SiO_2 conduction band and p-type Si is $E_{Si} = 4.3$ eV, graphene is $E_g = 3.66$ eV, and charge-trap sites in the gate oxide is $E_b = 2.58-2.64$ eV. (b) Carrier concentration (n) relaxation of an 8-μm-long GFET ($V_{bg} = 0$ V) as a function of time (blue scattered points) after a 442 nm laser-irradiation-induced charge-ejecting process from the gate oxide. The theoretical calculation result of the trapped-charge density relaxation is the red dashed curve.

is delivered independently at the same intensity of 600 μW onto a 40-μm-long GFET, as shown in Figure 5a. First, we apply an electrical gate voltage ($V_{bg} = -50$ V) without laser irradiation. After 60 s, each focused laser irradiates the center of the GFET. For $V_{bg} < V_{Dirac}$, the graphene channel is nominally p-type. After ejecting electrons from the charge trap sites in the gate oxide by laser irradiation, positively charged trap sites remain in the gate oxide. These positively charged trap sites induce n-type carriers in the graphene channel through capacitive coupling (gating effect) and lower the p-type carrier concentration of graphene ($V_{bg} < V_{Dirac}$), which increases the resistance incrementally, as shown in Figure 5a. When the GFET is irradiated with 2.81 eV (442 nm) instead of 1.96 eV (633 nm), the resistance change is relatively large. If the photothermal (laser-irradiation-induced heating) effect is the dominant charge-transfer mechanism in GFETs, the resistance

change should be similar in the case of the same intensity of laser irradiation. In addition, we also observe the laser-irradiation-induced doping effect in GFETs without any perpendicular electric field (applied gate voltage), as shown in Figure 4b and Figure S8, so a high electric-field-induced avalanche effect[46] cannot be the dominant charge-transfer mechanism. From these results, we strongly believe that the photon-energy-dependent mechanism dominates the resulting trapped-charge density and the doping effect in graphene.

Since the resistance change in Figure 5a could be a combined result of charge-ejection and photocurrent effects, we measure the resistance of the graphene channel as a function of time after turning off the 442 nm laser, as shown in Figure 5b. This allows us to explore a genuine charge-carrier-density relaxation in the graphene channel and the energy-barrier height relative to the Fermi energy. Figure 5b shows the carrier concentration (n) of an 8-μm-long GFET as a function of time (scattered points). Here, we obtain n from the measured resistance change using $n = \sigma/e\mu$, where σ is the conductance per unit area of graphene and μ is the mobility of the GFET (approximately 1100 $cm^2\ V^{-1}\ s^{-1}$). The relaxation of the carrier density is mainly due to the electron transfer from graphene to the trap sites by a built-in electric field that arises from the charge trap sites.[23]

Now, we examine the relaxation process of the graphene channel carrier concentration. Here, we assume that the decrease in the carrier concentration in the graphene channel corresponds to the decrease in the trapped-charge density of the trap sites ($\Delta n = \Delta N_D$). If we assume that the charge trap sites are uniformly distributed below the graphene channel according to a simple model of charge trap sites with two different energy levels, the change in the total trapped-charge density during the relaxation process due to thermal excitation can be described as[47−49]

$$N_D(t) = n_s \exp(-k_s t) + n_d \exp(-k_d t) \qquad (2)$$

where n_s and n_d are the initial trapped-charge densities of shallow and deep trap sites, respectively, and k_s and k_d are the relaxation rate constants of those sites, respectively. The relaxation rate constant k_n is expressed as[47,48]

$$k_n = N_g v_{th} \sigma_c \exp(-E_b/k_B T) \qquad (3)$$

where N_g is the effective density of states in graphene, v_{th} is the thermal velocity of the charge, σ_c is the trapping cross section of the trap site (which is assumed to be approximately 3.1×10^{-13} cm^2),[50] E_b is the trap energy barrier relative to the Fermi energy, k_B is the Boltzmann constant, and T is room temperature. The result of the relaxation process calculation is well fitted (red dashed curve), as shown in Figure 5b. From the calculated fit to the data, we estimate two energy barriers relative to the Fermi energy of graphene: 1.02 and 1.08 eV. From the fitting results and the energy level difference of the graphene Dirac point and the bottom of the SiO_2 conduction band of $E_g = 3.66$ eV,[45] we can estimate that the energy levels of the trap sites relative to the bottom of the SiO_2 conduction band are $E_b = 2.58$ eV ≈ 2.64 eV (see the inset of Figure 5a). These results are consistent with our observation that the doping effect by 633 nm (1.96 eV) laser irradiation is suppressed compared to that of 442 nm (2.81 eV) irradiation, as shown in Figure 5a.

CONCLUSIONS

In conclusion, we have demonstrated that laser irradiation can induce spatially controllable p−n junctions in graphene devices without additional structures, such as extra local gates and chemical dopants. The focused laser ejects the trapped-charge carriers in the gate oxide and modifies the electrostatic potential of the substrate. From the electrical measurements, we observe the effects that range from large shifts in the Dirac voltage ($\Delta V_{Dirac} \approx -60$ V) to the double Dirac peak in graphene. Furthermore, from the gate-dependent SPM, we verify the formation of p−n−p and p−n−p−n−p junctions, and we observe that the stable and sharp p−n junctions formed by laser irradiation in the graphene due to the deep energy levels (~2.6 eV) of the trap sites in the gate oxide. This energy scale corresponds to ~470 nm wavelength light, which indicates that the charge-trap effect should be considered when a photodetector is designed in a range of 500−400 nm wavelength light.

On the other hand, this technique allows for control of the local doping location, concentration, physical size (0.5−10 μm), and number of p−n junctions in graphene by controlling the position, intensity, irradiation time, and wavelength of the focused laser without extra local gate, chemical treatment, and plasmonic structures. Thus, focused-laser manipulation of the induced p−n junctions in graphene with nanoscale floating gates can be applied to produce more stable and efficient graphene-based optoelectronic devices, such as the optical trigger nonvoltaic memory and high-efficiency energy-harvesting devices, but also can be useful in fundamental studies, such as studies of the periodic potential-induced quantum behavior in graphene.

METHODS

Sample Fabrication. The single-layer graphene is grown on 25 μm thick Cu foil (Alfa Aesar, 99.8%) by a plasma-enhanced chemical vapor deposition method at 700−830 °C using methane as both carbon and hydrogen source. Large-scale-grown graphene is transferred onto a SiO_2(300 nm)/Si(highly p-doped) substrate by etching the Cu foil with an aqueous solution of $FeCl_3$. Before Cu etching, graphene/Cu is spin-coated with PMMA (950K A2) for a mechanical supporting layer during the transfer process. After the Cu foils are dissolved completely, the PMMA/graphene

membranes are washed with DI water and transferred onto the SiO_2(300 nm)/Si(highly p-doped) substrate, and the PMMA is removed by acetone. We also prepared the mechanically exfoliated graphene from Kish graphite. From prepared single-layer graphene, graphene channels are patterned using an O_2 plasma process. After e-beam lithography and e-gun evaporation, the source and drain electrodes of Cr/Au (10/40 nm) are prepared on the graphene. The highly p-doped Si substrate is used as a global back-gate electrode.

Focused-Laser-Irradiation-Induced Doping and SPM Setup. Laser-induced doping and gate-dependent SPM images in the GFET are obtained using a home-built two-wavelength laser confocal optical setup with a 442 nm He−Cd laser (Kimmon Koha Co., Ltd.), 633 nm He−Ne laser (JDS Uniphase), dichroic mirror, and object lens (50X Mitutoyo Plan Apo SL). The 442 nm laser is used for the focused-laser-irradiation-induced doping effect on the GFET. Gate-dependent SPM images are obtained using a 633 nm laser and a lock-in technique. An optical chopper (SR540, Stanford Research Systems) modulated the 633 nm laser, and the modulated photocurrent from the GFET is measured by lock-in amplifier at 1.45 kHz (SR830, Stanford Research Systems).

Conflict of Interest: The authors declare no competing financial interest.

Acknowledgment. This research was supported by the Future-based Technology Development Program (Nano Fields) (2012-0006233) and the Basic Science Research Program (BSRP) (2013-030172) through the National Research Foundation of Korea (NRF) grant funded by the Korea government (MSIP) (2008-0061906). M.H.B. was supported by the Korea Research Institute of Standards and Science under the Project grant (13011041, 12073009). Y.S.K., J.H.L., and S.H.C. were supported by the Priority Research Centers Program (2012-0005859), the BSRP (2012-040278), the Center for Topological Matter in POSTECH (2012-0009194), and the Nanomaterial Technology Development Program (2012M3A7B4049888) through the NRF funded by MSIP. J.S. and J.R.A. were supported by the Research Center Program of Institute for Basic Science in Korea. The authors also wish to thank B. G. Shin for useful discussions. H.K. and S.W.L. were supported through BSRP (2012R1A2A2A01045496) and WCU (R31-2008-000-10057-0) programs supported by the NRF funded by MSIP.

Supporting Information Available: More detailed set of data for a large V_{Dirac} shift for various V_{bg} and laser intensities and for the resistance varying over time. The SPM image of the p−n−p−n−p junction in the GFET after two different focused spots of the 442 nm laser irradiation. Focused-laser irradiation effect in mechanically exfoliated graphene with zero gate voltage. Fabrication procedures of suspended graphene. This material is available free of charge *via* the Internet at http://pubs.acs.org.

REFERENCES AND NOTES

1. Novoselov, K. S.; Geim, A. K.; Morozov, S. V.; Jiang, D.; Zhang, Y.; Dubonos, S. V.; Grigorieva, I. V.; Firsov, A. A. Electric Field Effect in Atomically Thin Carbon Films. *Science* **2004**, *306*, 666–669.
2. Zhang, Y.; Tan, Y. W.; Stormer, H. L.; Kim, P. Experimental Observation of the Quantum Hall Effect and Berry's Phase in Graphene. *Nature* **2005**, *438*, 201–204.
3. Nair, R. R.; Blake, P.; Grigorenko, A. N.; Novoselov, K. S.; Booth, T. J.; Stauber, T.; Peres, N.; Geim, A. K. Fine Structure Constant Defines Visual Transparency of Graphene. *Science* **2008**, *320*, 1308.
4. Chen, C.; Rosenblatt, S.; Bolotin, K. I.; Kalb, W.; Kim, P.; Kymissis, I.; Stormer, H. L.; Heinz, T. F.; Hone, J. Performance of Monolayer Graphene Nanomechanical Resonators with Electrical Readout. *Nat. Nanotechnol.* **2009**, *4*, 861–867.
5. Zhang, Y.; Brar, V. W.; Girit, Ç.; Zettl, A.; Crommie, M. F. Origin of Spatial Charge Inhomogeneity in Graphene. *Nat. Phys.* **2009**, *5*, 722–726.
6. Chen, J. H.; Jang, C.; Adam, S.; Fuhrer, M. S.; Williams, E. D.; Ishigami, M. Charged-Impurity Scattering in Graphene. *Nat. Phys.* **2008**, *4*, 377–381.
7. Martin, J.; Akerman, N.; Ulbricht, G.; Lohmann, T.; Smet, J. H.; von Klitzing, K.; Yacoby, A. Observation of Electron-Hole Puddles in Graphene Using a Scanning Single-Electron Transistor. *Nat. Phys.* **2007**, *4*, 144–148.
8. Cheianov, V. V.; Fal'Ko, V.; Altshuler, B. L. The Focusing of Electron Flow and a Veselago Lens in Graphene p-n Junctions. *Science* **2007**, *315*, 1252–1255.
9. Young, A. F.; Kim, P. Quantum Interference and Klein Tunnelling in Graphene Heterojunctions. *Nat. Phys.* **2009**, *5*, 222–226.
10. Park, C.-H.; Yang, L.; Son, Y.-W.; Cohen, M. L.; Louie, S. G. Anisotropic Behaviours of Massless Dirac Fermions in Graphene under Periodic Potentials. *Nat. Phys.* **2008**, *4*, 213–217.
11. Mueller, T.; Xia, F.; Avouris, P. Graphene Photodetectors for High-Speed Optical Communications. *Nat. Photonics* **2010**, *4*, 297–301.
12. Bonaccorso, F.; Sun, Z.; Hasan, T.; Ferrari, A. C. Graphene Photonics and Optoelectronics. *Nat. Photonics* **2010**, *4*, 611–622.
13. Sun, D.; Aivazian, G.; Jones, A. M.; Ross, J. S.; Yao, W.; Cobden, D.; Xu, X. Ultrafast Hot-Carrier-Dominated Photocurrent in Graphene. *Nat. Nanotechnol.* **2012**, *7*, 114–118.
14. Miao, X.; Tongay, S.; Petterson, M. K.; Berke, K.; Rinzler, A. G.; Appleton, B. R.; Hebard, A. F. High Efficiency Graphene Solar Cells by Chemical Doping. *Nano Lett.* **2012**, *12*, 2745–2750.
15. Gabor, N. M.; Song, J. C. W.; Ma, Q.; Nair, N. L.; Taychatanapat, T.; Watanabe, K.; Taniguchi, T.; Levitov, L. S.; Jarillo-Herrero, P. Hot Carrier-Assisted Intrinsic Photoresponse in Graphene. *Science* **2011**, *334*, 648–652.
16. Echtermeyer, T. J.; Britnell, L.; Jasnos, P. K.; Lombardo, A.; Gorbachev, R. V.; Grigorenko, A. N.; Geim, A. K.; Ferrari, A. C.; Novoselov, K. S. Strong Plasmonic Enhancement of Photovoltage in Graphene. *Nat. Commun.* **2011**, *2:458*, doi: 10.1038/ncomms1464.
17. Hong, A. J.; Song, E. B.; Yu, H. S.; Allen, M. J.; Kim, J.; Fowler, J. D.; Wassei, J. K.; Park, Y.; Wang, Y.; Zou, J.; *et al.* Graphene Flash Memory. *ACS Nano* **2011**, *5*, 7812–7817.
18. Kim, S.-M.; Song, E. B.; Lee, S.; Zhu, J.; Seo, D. H.; Mecklenburg, M.; Seo, S.; Wang, K. L. Transparent and Flexible Graphene Charge-Trap Memory. *ACS Nano* **2012**, *6*, 7879–7884.
19. Lee, S.; Song, E. B.; Kim, S.; Seo, D. H.; Seo, S.; Won Kang, T.; Wang, K. L. Impact of Gate Work-Function on Memory Characteristics in Al_2O_3/HfO_x/Al_2O_3/Graphene Charge-Trap Memory Devices. *Appl. Phys. Lett.* **2012**, *100*, 023109.
20. Rao, G.; Freitag, M.; Chiu, H.-Y.; Sundaram, R. S.; Avouris, P. Raman and Photocurrent Imaging of Electrical Stress-Induced p-n Junctions in Graphene. *ACS Nano* **2011**, *5*, 5848–5854.
21. Estrada, D.; Dutta, S.; Liao, A.; Pop, E. Reduction of Hysteresis for Carbon Nanotube Mobility Measurements Using Pulsed Characterization. *Nanotechnology* **2010**, *21*, 085702.
22. Buchanan, D. A.; Fischetti, M. V.; DiMaria, D. J. Coulombic and Neutral Trapping Centers in Silicon Dioxide. *Phys. Rev. B* **1991**, *43*, 1471.
23. Williams, R. Photoemission of Electrons from Silicon into Silicon Dioxide. *Phys. Rev.* **1965**, *140*, A569–A575.
24. Lundstrom, I.; Svensson, C. Tunneling to Traps in Insulators. *J. Appl. Phys.* **1972**, *43*, 5045–5047.
25. Imam, S. A.; Deshpande, T.; Guermoune, A.; Siaj, M.; Szkopek, T. Charge Transfer Hysteresis in Graphene Dual-Dielectric Memory Cell Structures. *Appl. Phys. Lett.* **2011**, *99*, 082109.
26. Liao, Z. M.; Han, B. H.; Zhou, Y. B.; Yu, D.-P. Hysteresis Reversion in Graphene Field-Effect Transistors. *J. Chem. Phys.* **2010**, *133*, 044703.
27. Myung, S.; Park, J.; Lee, H.; Kim, K. S.; Hong, S. Ambipolar Memory Devices Based on Reduced Graphene Oxide and Nanoparticles. *Adv. Mater.* **2010**, *22*, 2045–2049.

28. Wang, D.; Liu, X.; He, L.; Yin, Y.; Wu, D.; Shi, J. Manipulating Graphene Mobility and Charge Neutral Point with Ligand-Bound Nanoparticles as Charge Reservoir. *Nano Lett.* **2010**, *10*, 4989–4993.
29. Guo, B.; Liu, Q.; Chen, E.; Zhu, H.; Fang, L.; Gong, J. R. Controllable N-Doping of Graphene. *Nano Lett.* **2010**, *10*, 4975–4980.
30. Kim, B. H.; Hong, S. J.; Baek, S. J.; Jeong, H. Y.; Park, N.; Lee, M.; Lee, S. W.; Park, M.; Chu, S. W.; Shin, H. S. N-Type Graphene Induced by Dissociative H_2 Adsorption at Room Temperature. *Sci. Rep.* **2012**, *2*, 690.
31. Sun, J. T.; Lu, Y. H.; Chen, W.; Feng, Y. P.; Wee, A. T. S. Linear Tuning of Charge Carriers in Graphene by Organic Molecules and Charge-Transfer Complexes. *Phys. Rev. B* **2010**, *81*, 155403.
32. Chiu, H. Y.; Perebeinos, V.; Lin, Y. M.; Avouris, P. Controllable p-n Junction Formation in Monolayer Graphene Using Electrostatic Substrate Engineering. *Nano Lett.* **2010**, *10*, 4634–4639.
33. Yan, J.; Kim, M.-H.; Elle, J. A.; Sushkov, A. B.; Jenkins, G. S.; Milchberg, H. M.; Fuhrer, M. S.; Drew, H. D. Dual-Gated Bilayer Graphene Hot-Electron Bolometer. *Nat. Nanotechnol.* **2012**, *7*, 472–478.
34. Park, J.; Ahn, Y. H.; Ruiz-Vargas, C. Imaging of Photocurrent Generation and Collection in Single-Layer Graphene. *Nano Lett.* **2009**, *9*, 1742–1746.
35. Xia, F.; Mueller, T.; Golizadeh-Mojarad, R.; Freitag, M.; Lin, Y.-M.; Tsang, J.; Perebeinos, V.; Avouris, P. Imaging of Photocurrent Generation and Collection in Single-Layer Graphene. *Nano Lett.* **2009**, *9*, 1039–1044.
36. Xu, X.; Gabor, N. M.; Alden, J. S.; van der Zande, A. M.; Mceuen, P. L. Photo-Thermoelectric Effect at a Graphene Interface Junction. *Nano Lett.* **2010**, *10*, 562–566.
37. Kim, Y. S.; Lee, J. H.; Kim, Y. D.; Jerng, S.-K.; Joo, K.; Kim, E.; Jung, J.; Yoon, E.; Park, Y. D.; Seo, S.; *et al.* Methane as an Effective Hydrogen Source for Single-Layer Graphene Synthesis on Cu Foil by Plasma Enhanced Chemical Vapor Deposition. *Nanoscale* **2013**, *5*, 1221–1226.
38. Kim, M.; Yoon, H. A.; Woo, S.; Yoon, D.; Lee, S. W.; Cheong, H. Polarization Dependence of Photocurrent in a Metal-Graphene-Metal Device. *Appl. Phys. Lett.* **2012**, *101*, 073103.
39. Song, J. C. W.; Rudner, M. S.; Marcus, C. M.; Levitov, L. S. Hot Carrier Transport and Photocurrent Response in Graphene. *Nano Lett.* **2011**, *11*, 4688–4692.
40. Freitag, M.; Low, T.; Xia, F.; Avouris, P. Photoconductivity of Biased Graphene. *Nat. Photonics* **2012**, *7*, 53–59.
41. Bae, M.-H.; Ong, Z.-Y.; Estrada, D.; Pop, E. Imaging, Simulation, and Electrostatic Control of Power Dissipation in Graphene Devices. *Nano Lett.* **2010**, *10*, 4787–4793.
42. Dorgan, V. E.; Bae, M.-H.; Pop, E. Mobility and Saturation Velocity in Graphene on SiO_2. *Appl. Phys. Lett.* **2010**, *97*, 082112.
43. Powell, R. J.; Berglund, C. N. J. Photoinjection Studies of Charge Distributions in Oxides of MOS Structures. *Appl. Phys.* **1971**, *42*, 4390–4397.
44. Powell, R. J. Interface Barrier Energy Determination from Voltage Dependence of Photoinjected Currents. *J. Appl. Phys.* **1970**, *41*, 2424.
45. Yan, R.; Zhang, Q.; Li, W.; Calizo, I.; Shen, T.; Richter, C. A.; Hight-Walker, A. R.; Liang, X.; Seabaugh, A.; Jena, D. Determination of Graphene Work Function and Graphene-Insulator-Semiconductor Band Alignment by Internal Photoemission Spectroscopy. *Appl. Phys. Lett.* **2012**, *101*, 022105–022105−4.
46. Woods, M. H. Hole Traps in Silicon Dioxide. *J. Appl. Phys.* **1976**, *47*, 1082.
47. DiMaria, D. J.; Stasiak, J. W. Trap Creation in Silicon Dioxide Produced by Hot Electrons. *J. Appl. Phys.* **1989**, *65*, 2342.
48. Chen, G.; Xu, Z. Charge Trapping and Detrapping in Polymeric Materials. *J. Appl. Phys.* **2009**, *106*, 123707–123707−5.
49. Lee, Y. G.; Kang, C. G.; Jung, U. J.; Kim, J. J.; Hwang, H. J.; Chung, H.-J.; Seo, S.; Choi, R.; Lee, B. H. Fast Transient Charging at the Graphene/SiO_2 Interface, Causing Hysteretic Device Characteristics. *Appl. Phys. Lett.* **2011**, *98*, 183508.
50. Ning, T. H. Capture Cross Section and Trap Concentration of Holes in Silicon Dioxide. *J. Appl. Phys.* **1976**, *47*, 1079–1081.